CrystEngComm

ARTICLE

Switching of the products by size and shape of catalytic nanoparticles during CVD growth of MoS_2 nanotubes

Received 00th January 20xx,
Accepted 00th January 20xx

DOI: 10.1039/x0xx00000x

www.rsc.org/

Weng Mengting,[a] Takashi Yanase,[a] Fumiya Uehara,[a] Sho Watanabe,[a] Takuya Miura,[a] Taro Nagahama[a] and Toshihiro Shimada[a]

Nanowires of layered materials are important because the highest sensitivity as electrically-detected chemical sensors is expected. MoS_2 nanowires have been synthesized by the catalytic chemical vapor deposition method on silicon substrates drop-coated with FeO nanoparticles of different shapes. Switching of the products (MoS_2 nanowires to SiO_2 nanowires) has been observed when the shapes and sizes of the FeO nanoparticles changed. MoS_2 nanowires were grown in the presence of six-horned octahedral nanoparticles, whereas SiO_2 nanowires were formed in the presence of spherical nanoparticles. The morphology, crystal structure and elemental composition have been fully investigated to elucidate the growth mechanism of the nanowires. The kinetics of the grown SiO_2 and MoS_2 nanowires is competing, giving rise to the observed switching.

Introduction

Semiconductor nanowires have been a hot topic over the past decades. One of their major applications is in nanoscale sensor arrays, which is important, for example, as the interface between a bio-system and information technologies.[1, 2] The sensitivity of the nano-sensors depends on the capping layer on the surfaces, which is primarily introduced for the protection of the semiconductor from the surrounding solution or atmosphere. The capping layer can also be used to provide a selectivity to the sensing species. For the conventional semiconductors, such as Si or GaAs, the surface is chemically active and has to be capped by oxides or organic species, which sometimes reduces their sensitivity, and the long-term stability is still problematic. The highest sensitivity and stability is expected from the layered materials such as graphene and transition metal dichalcogenides (TMDs). Graphene can be made into nanowires, *i.e.*, carbon nanotubes, and their application in nanoscale sensors is promising.[3-5] However, the physical property of carbon nanotubes is strongly dependent on their chirality that is difficult to control.[6, 7] Therefore, it is worth studying the nanotubes of TMDs, in which no strong chirality effects have been reported.

Molybdenum dioxide (MoS_2), a representative TMD material, has a broad range of applications including field effect transistors (FET),[8-10] gas sensors,[11-13] lithium batteries[14-16] and solar cells.[17-20] Several methods have been used to grow MoS_2 nanowires, such as the vapor transport reaction with MoS_2 powders,[21, 22] H_2S reduction of molybdenum oxides mixtures,[23] thermal decomposition of the precursor $(NH_4)_2MoS_4$ using the template method,[24] hydrothermal treatment of $LiMoS_2$ lamella,[25] and sulfurization of the precursor $Mo_6S_4I_6$ nanowires.[26] Nevertheless, progress towards the control of the nanowires growth has still been limited. It is necessary to investigate the mechanism for their growth process to control the size of the nanowires and optimize their properties.

In this paper, we focus on the chemical vapor deposition (CVD) with solid catalyst nanoparticles of MoS_2 nanowires. This approach is successful for the growth of carbon nanotubes, Si, GaAs and ZnO. In our previous study, it was found that FeO and other metal oxides can function as catalysts for the growth of the MoS_2 nanotubes.[27] In this study, we focus on the impact of the size and shape of the chemically synthesized FeO nanoparticles on the nanowire growth.

FeO is one of the common iron oxides, which consist of goethite (α-FeOOH), hematite (α-Fe_2O_3), magnetite (Fe_3O_4), maghemite (γ-Fe_2O_3) etc. Among them, FeO is the most chemically reactive, as a result of its defective NaCl structure which is non-stoichiometric with an O-vacancy.[28] As reported, Sun's group has synthesized FeO nanoparticles with two shapes, *i.e.*, octahedral and spherical.[29] It is of great interest to investigate whether the shape has an effect on the catalytic reactivity of the FeO nanoparticles. Actually, we found switching of the products from MoS_2 and SiO_2 as described in the following sections.

Results and Discussion

[a] Division of Applied Chemistry, Faculty of Engineering, Hokkaido University, Kita 13 Nishi 8, Kita-ku, Sapporo 060-8628, Japan.
[b] (ESI) available: See DOI: 10.1039/x0xx00000x

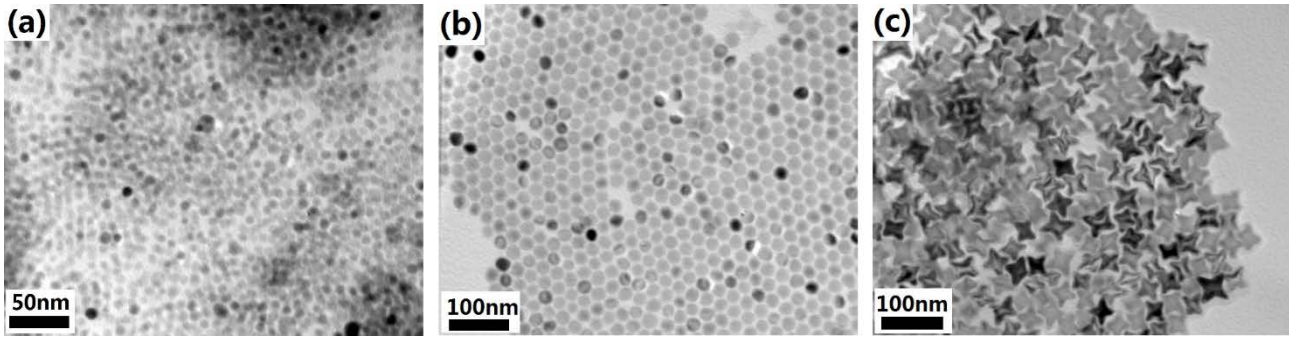

Fig.1 TEM images of FeO nanoparticles: (a) 9 nm, (b) 24 nm spherical and (c) 30 nm six-horned octahedral nanoparticles.

Figure 1 shows the typical TEM images of the synthesized FeO nanoparticles. As already reported [29], the shapes and sizes of the particles are controlled by changing the reaction conditions. In this study, we synthesized 9 nm spherical nanoparticles (Figure 1(a)) by heating the mixture of iron(III) acetylacetonate [$Fe(acac)_3$], oleic acid (OA) (4 ml) and oleylamine (OAm) (6 ml) at 220 ^{o}C, then at 300 ^{o}C, each for 30 min. Under the same conditions, 30 nm six-horned octahedral nanoparticles (Figure 1(c)) were acquired by the decomposition of $Fe(acac)_3$ mixed with OA (5.5 ml) and OAm (5 ml).

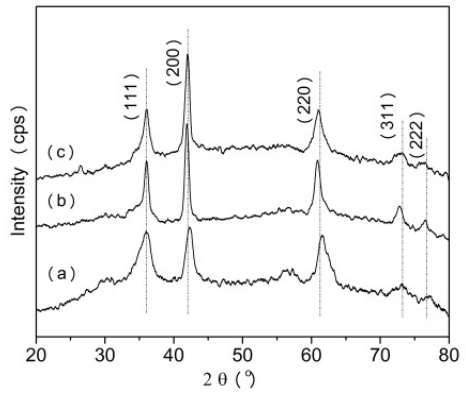

Fig. 2 XRD patterns of FeO nanoparticles: (a) 9 nm, (b) 24 nm and (c) 30 nm nanoparticles.

Additionally, we found that stirring is another essential factor to control the shape of the particles during the decomposition. For example, heating a mixture of $Fe(acac)_3$, OA (5.5 ml) and OAm (5 ml) without stirring at 220 ^{o}C for 1h, then at 300 ^{o}C for 30 min, formed 50 nm six-horned octahedral nanoparticles (Figure S1), whereas 24 nm spherical nanoparticles (Figure 1(b)) were obtained by continuous stirring. The flow chart of the synthesis process is shown in Figure S2.

The crystal structures of the 9 nm and 24 nm spherical particles and 30 nm six-horned octahedral particles were characterized by XRD, as shown in Figure 2. It is clear that all the samples exhibit the 111, 200, 220, 311 and 222 characteristic peaks of the FeO structure, indicating that the synthesized nanoparticles are almost pure FeO. Raman were also taken, as shown in Figure S3. The morphologies of the nanoparticles heated to 1000 ^{o}C on SiO_2/Si substrates are shown in Figure S4, and their corresponding Raman spectra and XRD are shown in Figure S5 and S6. Even though some morphology change has occurred to the nanoparticles due to their agglomeration at the high temperature, it is obvious that the size and shape of the nanoparticles are distinct from each other. We admit that very thin residual carbon might exist on the surface of catalysts, but the coverage of the carbon is the same for all the catalysts.

The nanowires were grown on 285 nm SiO_2/Si substrates in a CVD reactor made of quartz tube (Figure S7)[30,31] at 1000 ^{o}C with MoO_3 and S using the 9 nm, 24 nm spherical, 30 nm and 50 nm six-horned octahedral particles as catalysts. Powders of 0.15g MoO_3 and 1.5g S were evaporated at 650 ^{o}C and 280 ^{o}C, respectively. The gas flow of MoO_3 and S lines were started when the temperature reached 1000 ^{o}C. The pressure in the growth tube was 1 atm and the growth time was 1 hour.

The SEM images of the products after CVD using the 9 nm, 24 nm, 30 nm and 50 nm FeO are shown in Figures 3 (a), (b), (c) and S8 respectively. TEM equipped with EDS was employed to investigate their crystal structures and morphologies, as shown in Figure 4. In the case of the 9 nm spherical catalyst particles, high-aspect ratio nanowires with a diameter of 40 nm and length of 10 μm, were found to grow in a high density. The EDS and diffraction results show that they are amorphous SiO_2 nanowires with a particle cap. The EDS analysis revealed that the particles consist of Mo, Fe and S.

When the diameter of the spherical particles increased to 24 nm, as shown in Figure 3(b), low-density nanowires and particles

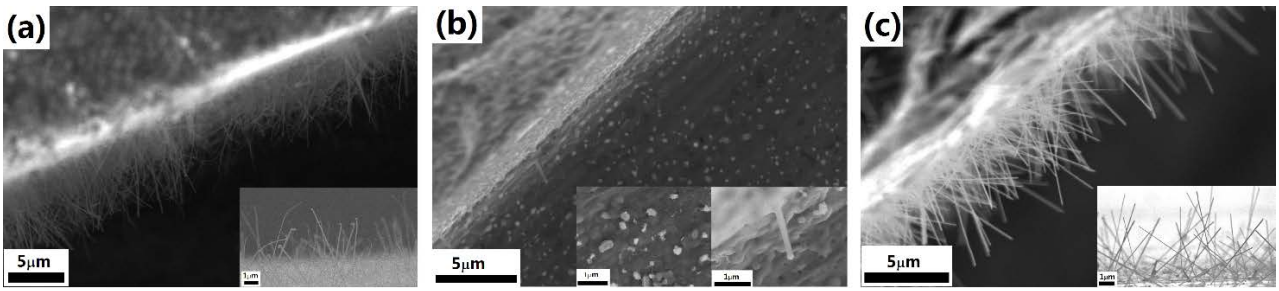

Fig. 3 SEM images after CVD with (a) 9 nm, (b) 24 nm and (c) 30 nm catalyst nanoparticles.

covered by MoS_2 films were observed. Similar to the ones grown with the 9 nm particles, a particle can be found at the tip of a nanowire (Figure 3b inset). From the Raman spectra and EDS results, the nanowires were SiO_2. Compared to Figure 3(a), the diameter of the nanowire increased and the length became shorter.

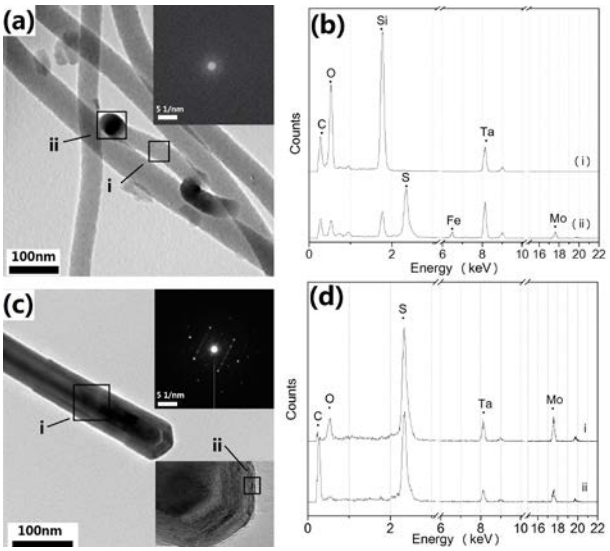

Fig. 4 TEM images of (a) SiO_2 and (c) MoS_2 nanowires. (b) and (d) are the EDS results corresponding to (a) and (c),respectively.

When the shape of the catalyst nanoparticles changed from spherical to 30 nm six-horned octahedra, nanowires with no particle caps were found (Figure S9). The nanowires are typically a few micrometers in length with diameters from 40 to 80 nm. Based on the EDS, they were composed of Mo and S. The peaks in the TEM diffraction (Figure 4(c) inset) and Raman spectra (Figure S10) of the nanowires correspond to those of MoS_2. The two peaks in the Raman spectra, centered at 380 and 406 cm^{-1}, were assigned as the E_{2g} and A_{1g} modes, respectively.[32-34] In the case of 50 nm, low-density MoS_2 nanowires were obtained (Figure S8), which were evidenced by TEM-EDS (Figure S11).

We have now observed drastic switching of the CVD product depending on the size and shape of the FeO nanoparticle catalysts. This result is summarized in the first row of Table 1. In order to study the growth mechanism, CVD experiments with only flowing MoO_3 (no S) were conducted. The SEM images are shown in Figure S12, and no nanowires were observed in them. Instead, the particles randomly dispersed on the substrates.

These products were characterized by Raman spectroscopy. Figures 5 (a), (b) and (c) are the results of using the 9 nm, and 24 nm spherical and 30 six-horned octahedral catalysts, respectively. In the 9 nm case, peaks of both MoO_2 and FeO_x (x=1, 3/2, 4/3) were found in contrast to the one of the 24 nm spherical nanoparticles, in which no MoO_2 peaks could be found, indicating that MoO_3 could be deposited on the smaller spherical particles. When the shape of the particles changed to six-horned octahedra, significant peaks of MoO_2 could be observed, as shown in Figure 5(c). It is proposed that the sharp edges and acute angles in the six-horned octahedra contribute to the deposition of MoO_3.

Based on the results of the above experiments summarized in Table 1, the growth mechanism can be described as follows.

Although SiO_2 has a very low vapour pressure at 1000 °C, SiO can be vaporized under reducing conditions from the substrate surface and furnace wall. We suggest that based on the reaction $SiO_2 + S \rightarrow SiO + SO_2$, SiO (~1.33 Pa, 1000 °C) [37] is the source of the SiO_2 nanowires. The MoO_3 vapor pressure in the furnace is estimated to be 4 Pa, which is described in the supporting information. Based on this value, the competition between the SiO and MoO_3 vapor gives rise to the formation of two different nanowires with the assistance of the different shapes of the catalyst nanoparticles, as illustrated in Figure 6.

Table 1. Summary of the CVD products.

Catalysts (FeO particles)	9 nm sphere	24 nm sphere	30nm truncated octahedra
Growth of nanowires (MoO_3 and S flow)	SiO_2 nanowires	few SiO_2 nanowires	MoO_3 nanowires
MoO_2 Raman peaks (only MoO_3 flow)	weak	none	strong

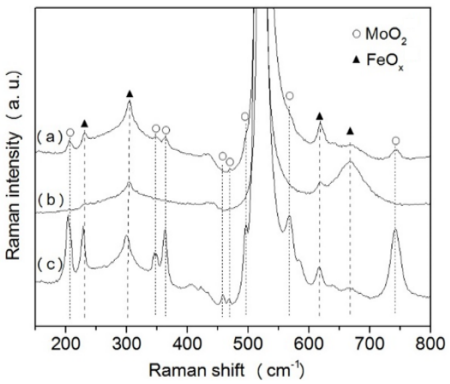

Fig. 5 Raman spectra after CVD with (a) 9-nm spherical FeO+MoO_3, (b) 24-nm spherical FeO+MoO_3 and (c) 30-nm six-horned octahedral FeO + MoO_3. Raman peaks were identified using Refs. 35 and 36.

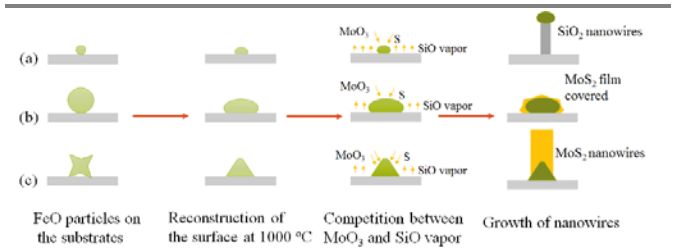

Fig. 6 Mechanism of switching between SiO_2 and MoS_2.

By using 9-nm particles, the particles consisting of Mo, Fe and S were observed at the top of the SiO_2 nanowires, indicating that the SiO_2 nanowire growth proceeded through a vapor-liquid-solid (VLS) or vapor-solid-solid (VSS) mechanism.[38-42] In the VSS mechanism, the growth temperature is lower than the eutectic temperature (50-90% of the reported eutectic temperature) and more facets of the catalysts at the top would be observed due to the lower solubility of the precursor atoms.[41, 42] The round particle shape of the catalyst existing at the top of the nanowire in Figure 4(a) illustrates that the growth of the SiO_2 nanowire is not explained by the VSS mechanism. The reaction temperature at 1000 °C, higher

than the eutectic point (≤ 940 °C, because of the size effect) in the FeO-FeS system,[43, 44] makes it possible to explain it by the VLS mechanism. At 1000°C, Ar gas carrying MoO_3 and sulfur from the low-temperature region starts to flow, depositing Mo, O and S atoms onto the particles. Some sulfur atoms react with FeO, leading to the formation of the FeO-FeS system. When the FeS content in the particle reached a certain value, a liquid alloy drop will be formed. Whereas MoO_3 tends to quickly evaporate rather than diffuse into the particles. Additionally, an experiment without MoO_3 (only S) was also conducted, as shown in Figure S13. SiO_2 nanowires did not grow in this case, which demonstrates that the Mo absorbed into the drop played an important role in its catalyzing effect.

With the increasing size of the nanoparticles, the growth of the SiO_2 nanowires seems to become more difficult. As shown in Figure 3(b), lower-density nanowires were found compared with Figure 3(a). With the increasing size of the nanoparticles, the surface to volume ratio decreased, leading to fewer active sites for interaction with the chemical adsorbate.[45] Thus, the absorbance of the S, MoO_3, SiO become lower than that in the smaller particles. For example, as shown in Figure 5(b) and Table 1, compared with the weak peaks in the 9 nm particles, no MoO_x peaks were found in the case of the larger particles. However, due to the increased volume of the particles, more atoms need to be absorbed to grow SiO_2 nanowires by the VLS mechanism. In other words, it required a longer time to form the supersaturated alloy drop, whereas at the same time, MoS_2 thin films are formed with the presence of the MoO_3 and S vapors, which is not affected by the nanoparticles. Thus, less SiO_2 nanowires were formed as the size of the nanoparticles increased, instead, the particles tended to be covered by the MoS_2 thin films.

When the shape of the catalyst nanoparticles changed from spherical to six-horned octahedra, MoS_2 nanowires were formed. Unlike the SiO_2 nanowires, no particle cap at the tip of the MoS_2 nanowires were ever found, indicating that the mechanism of MoS_2 cannot be the VLS mechanism. As the temperature increased to 1000 °C, six-horned octahedral FeO nanoparticles start forming frustums, as shown in Figure S4(c). The sharp edges and acute angles of which contribute the deposition of MoO_3 (Figure 5(c) and Table 1). At a high temperature, an oxygen deficiency in the deposited MoO_3 would occur,[46, 47] which can be incorporation sites for sulfur atoms, leading to the nucleation of MoS_2. With the orientation effect of the sharp edges of the catalyst, MoS_2 nanowires were then formed. Thus, we suggest that the mechanism of the MoS_2 nanowires is the VS mechanism. Compared with the VLS mechanism of SiO_2 nanowires, the MoS_2 nanowires with the VS mechanism can be understood as a simple surface reaction system, while the mechanism of the SiO_2 nanowire growth is more complex because it involves diffusion and precipitation of silicon atoms into the alloy drops. Additionally, when the nanoparticle size increased to 50 nm, lower-density MoS_2 nanowires were grown, indicating that the increase in the size of nanoparticles slowed down the growth of MoS_2 nanowires.

Conclusions

In this study, high-aspect-ratio MoS_2 and SiO_2 nanowires have been successfully fabricated by catalytic CVD, in which FeO nanoparticles with different and well-defined shapes were used as catalysts. It was found that switching of the composition of the nanowires occurred when the shapes of the nanoparticle catalysts changed. In the case of spherical nanoparticles, high-density SiO_2 nanowires were fabricated, whereas in the case of six-horned octahedral nanoparticles, MoS_2 nanowires were formed. This switching can be explained by the competition between the growth of the SiO_2 nanowires by the VLS mechanism and MoS_2 nanowires grown by the VS mechanism. The deposition of MoO_2 species on the catalyst seems critical in controlling the process.

Experimental

Synthesis

Catalysts. FeO nanoparticles were synthesized by the thermal decomposition of iron (III) acetylacetonate [$Fe(acac)_3$] (99.9%, Sigma-Aldrich), according to a previous report.[29] Briefly, 0.7g $Fe(acac)_3$ was mixed with either 4 ml oleic acid (OA), 6ml oleylamine (OAm) or 5ml OA and 5ml OAm. The solutions were heated at 220 °C and 300 °C under Ar (99.9999%) for 1-2h to yield FeO nanoparticle solutions with different sizes and shapes. The flow chart is shown in the supporting information of Figure S2.

Nanowires. MoS_2 nanowires were grown using a CVD apparatus, as shown in the supporting information. The furnace tube had a 28-mm diameter and separated into three zones; zones A, B and C. MoO_3 (99.5%)) and S powders were purchased from Kanto Chemistry. MoO_3 (0.15g) was placed into a quartz tube in zone A, and the S powders (1.5 g) were placed in an alumina boat in another heating apparatus.

Si wafers with 500 nm SiO_2 layers were drop-coated with the catalyst FeO solution (0.1 mmol/L) after RCA cleaning. The substrates were then transferred to zones B and C of the tube furnace. In typical experiments, after the furnace and S apparatus were heated to the set temperature, the Ar gases carrying the MoO_3 (40 sccm) and S (800 sccm) were flowed into the furnace. The temperatures of the zones were 280 °C for the sulfur source, 650 °C in zone A, and 1000 °C in zones B and C. After holding the temperature for 1 h, the furnace were naturally cooled to room temperature. The experiment was conducted under atmospheric pressure.

Characterization

The FeO catalyst nanoparticles and MoS_2 nanowires have been characterized by a 200 kV JEOL JEM-2010 transmission electron microscope (TEM) equipped with an energy-dispersive (EDS) analyzer. The crystallinity of the nanoparticles were examined by a Rigaku Rint Ultima 2000 X-ray diffractometer (XRD) using Cu Kα radiation (λ= 0.1541 nm). The morphology of the nanowires was characterized by a JSV-6510LA scanning electron microscope (SEM) and JSM-6500F field emission scanning electron microscope (FE-

SEM). Raman spectroscopy (Renishaw Invia) with 532 nm excitation was used.

Acknowledgements

The present work is partly supported by CREST-JST grant. Instrumental analysis was supported by Nanotechonology platform at Hokkaido University by METI, Japan.

Notes and references

1 B. Tian, P. Xie, T. J. Kempa, D. C. Bell and C. M. Lieber, *Nat Nanotechnol*, 2009, **4**, 824-829.
2 B. Tian, T. Cohen-Karni, Q. Qing, X. Duan, P. Xie and C. M. Lieber, *Science*, 2010, **329**, 830-834.
3 J. Wang and M. Musameh, *Anal Chem*, 2003, **75**, 2075-2079.
4 M. G. Zhang, A. Smith and W. Gorski, *Anal Chem*, 2004, **76**, 5045-5050.
5 R. J. Chen, H. C. Choi, S. Bangsaruntip, E. Yenilmez, X. W. Tang, Q. Wang, Y. L. Chang and H. J. Dai, *J Am Chem Soc*, 2004, **126**, 1563-1568.
6 F. Yang, X. Wang, D. Zhang, J. Yang, D. Luo, Z. Xu, J. Wei, J. Wang, Z. Xu, F. Peng, X. Li, R. Li, Y. Li, M. Li, X. Bai, F. Ding and Y. Li, *Nature*, 2014, **510**, 522-524.
7 F. Qin, W. Shi, T. Ideue, M. Yoshida, A. Zak, R. Tenne, T. Kikitsu, D. Inoue, D. Hashizume and Y. Iwasa, *Nat. Commun.*, 2017, 14465.
8 B. Radisavljevic, A. Radenovic, J. Brivio, V. Giacometti and A. Kis, *Nat. Nanotechnol.*, 2011, **6**, 147-150.
9 S. Das, H. Chen, A. V. Penumatcha and J. Appenzeller, *Nano. Lett.*, 2013, **13**, 100-105.
10 D. Sarkar, W. Liu, X. Xie, A. C. Anselmo, S. Mitragotri and K. Banerjee, *ACS Nano*, 2014, **8**, 3992-4003.
11 H. Li, Z. Yin, Q. He, H. Li, X. Huang, G. Lu, D. W. H. Fam, A. I. Y. Tok, Q. Zhang and H. Zhang, *Small*, 2012, **8**, 63-67.
12 Q. He, Z. Zeng, Z. Yin, H. Li, S. Wu, X. Huang and H. Zhang, *Small*, 2012, **8**, 2994-2999.
13 B. Cho, M. G. Hahm, M. Choi, J. Yoon, A. R. Kim, Y. Lee, S. Park, J. Kwon, C. S. Kim, M. Song, Y. Jeong, K. Nam, S. Lee, T. J. Yoo, C. G. Kang, B. H. Lee, H. C. Ko, P. M. Ajayan and D. Kim, *Sci. Reports*, 2015, **5**, 8052.
14 C. Feng, J. Ma, H. Li, R. Zeng, Z. Guo and H. Liu, *Mater. Res. Bull.*, 2009, **44**, 1811-1815.
15 J. Xiao, D. Choi, L. Cosimbescu, P. Koech, J. Liu and J. P. Lemmon, *Chem. Mater.*, 2010, **22**, 4522-4524.
16 K. Chang and W. Chen, *ACS Nano*, 2011, **5**, 4720-4728.
17 M. Shanmugam, T. Bansal, C. A. Durcan and B. Yu, *Appl. Phys. Lett.*, 2012, **100**, 153901.
18 J. Lin, C. Chan and S. Chou, *Chem. Commun.*, 2013, **49**, 1440-1442.
19 M. Tsai, S. Su, J. Chang, D. Tsai, C. Chen, C. Wu, L. Li, L. Chen and J. He, *ACS Nano*, 2014, **8**, 8317-8322.
20 I. Jeon, D. Kutsuzawa, Y. Hashimoto, T. Yanase, T. Nagahama, T. Shimada and Y. Matsuo, *Org. Electron.*, 2015, **17**, 275-280.
21 M. Remskar, A. Mrzel, Z. Skraba, A. Jesih, M. Ceh, J. Demsar, P. Stadelmann, F. Levy and D. Mihailovic, *Science*, 2001, **292**, 479-481.
22 S. Fathipour, M. Remskar, A. Varlec, A. Ajoy, R. Yan, S. Vishwanath, S. Rouvimov, W. S. Hwang, H. G. Xing, D. Jena and A. Seabaugh, *Appl. Phys. Lett.*, 2015, **106**, 022114.
23 H. A. Therese, N. Zink, U. Kolb and W. Tremel, *Solid State Sci.*, 2006, **8**, 1133-1137.
24 E. M. Rivera-Munnoz, *J. Appl. Phys.*, 2007, **102**,094302.
25 V. Lavayen, N. Mirabal, C. O'Dwyer, M. A. Santa Ana, E. Benavente, C. M. Sotomayor Torres and G. Gonzalez, *Appl. Surf. Sci.*, 2007, **253**, 5185-5190.
26 M. Remskar, A. Mrzel, M. Virsek, M. Godec, M. Krause, A. Kolitsch, A. Singh and A. Seabaugh, *Nanoscale Res. Lett.*, 2011, **6**, 26.
27 M. Weng, T. Yanase, F. Uehara, S. Watanabe, T. Miura, Y. Hashimoto, T. Nagahama and T. Shimada, 2017, submitted.
28 R. M. Cornell and U. Schwertmann, *The iron oxides : structure, properties, reactions, occurrence, and uses.* VCH, Weinheim ; New York, 1996.
29 Y. Hou, Z. Xu and S. Sun, *Angew. Chem.*, 2007, **119**, 6445-6448.
30 T. Yanase, S. Watanabe, M. Weng, T. Nagahama and T. Shimada, J. Nanosci. Nanotech. 2016, **16**, 3223-3227.
31 T. Yanase, S. Watanabe, M. Weng, M. Wakeshima, Y. Hinatsu, T. Nagahama and T. Shimada, Crystal Growth & Design 2016, **16**, 4467–4472.
32 C. Lee, H. Yan, L. E. Brus, T. F. Heinz, J. Hone and S. Ryu, *ACS Nano*, 2010, **4**, 2695-2700.
33 H. Li, Q. Zhang, C. C. R. Yap, B. K. Tay, T. H. T. Edwin, A. Olivier and D. Baillargeat, *Adv. Funct. Mater.*, 2012, **22**, 1385-1390.
34 S. Sahoo, A. P. S. Gaur, M. Ahmadi, M. J. F. Guinel and R. S. Katiyar, *J. Phys. Chem. C*, 2013, **117**, 9042-9047.
35 M. Dieterle and G. Mestl, *Phys. Chem. Chem. Phys.*, 2002, **4**, 822-826.
36 D. de Faria, S. V. Silva and M. T. de Oliveira, *J. Raman Spectrosc.*, 1997, **28**, 873-878.
37 ULVAC Inc., *Vacuum Handbook*, Ohm-sha; Tokyo, 2002.
38 J. L. Elechiguerra, J. A. Manriquez and M. J. Yacaman, *Appl. Phys. A*, 2004, **79**, 461-467.
39 K. Kolasinski, *Current Opinion in Solid State and Materials Science*, 2006, **10**, 182-191.
40 Z. Xiao, L. Zhang, G. Meng, X. Tian, H. Zeng and M. Fang, *J. Phys. Chem. B*, 2006, **110**, 15724-15728.
41 J. L. Lensch-Falk, E. R. Hemesath, D. E. Perea and L. J. Lauhon, *J. Mater. Chem.*, 2009, **19**, 849-857.
42 C. Y. Wen, M. C. Reuter, J. Tersoff, E. A. Stach and F. M. Ross, *Nano Lett.*, 2010, **10**, 514-519.
43 S. J. Groves, J. Williamson and A. Sanyal, *Fuel*, 1987, **66**, 461-466.
44 M. C. Mayoral, M. T. Izquierdo, J. M. Andres and B. Rubio, *Thermochimica Acta*, 2002, **390**, 103-111.
45 B. R. Cuenya, *Thin Solid Films*, 2010, **518**, 3127-3150.
46 L. E. Firment and A. Ferretti, *Surf Sci.*, 1983, **129**, 155-176.
47 G. Mestl, C. Linsmeier, R. Gottschall, M. Dieterle, J. Find, D. Herein, J. J Ger, Y. Uchida and R. Schlogl, *Journal of Molecular Caralysis A: Chemical*, 2000, **162**, 463-492.